Effects of reflected electrons on the efficiency of high-power gyrotrons ⊕

Lea Marti ⓘ ; Ioannis Gr. Pagonakis ✉ ⓘ ; Chieh-Lin Chiang ⓘ ; Chuanren Wu ⓘ ; Jérémy Genoud ⓘ ;
Marthe Millen ⓘ ; Jean-Philippe Hogge ⓘ ; Alexander B. Barnes ⓘ

Check for updates

View
Online

Export
Citation

Articles You May Be Interested In

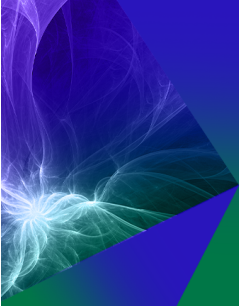Electron optics simulation in the overall gyrotron geometry

Phys. Plasmas (October 2024)

Megawatt power generation of the dual-frequency gyrotron for TCV at 84 and 126 GHz, in long pulses

AIP Conf. Proc. (September 2020)

A model of electron beam neutralization for gyrotron simulations

Phys. Plasmas (May 2024)

Effects of reflected electrons on the efficiency of high-power gyrotrons EP

Lea Marti,[1] Ioannis Gr. Pagonakis,[1,a] Chieh-Lin Chiang,[1] Chuanren Wu,[2] Jérémy Genoud,[3] Marthe Millen,[1] Jean-Philippe Hogge,[3] and Alexander B. Barnes[1]

AFFILIATIONS

[1]ETH Zürich, Institute of Molecular Physical Science (IMPS), CH-8093 Zürich, Switzerland
[2]Karlsruhe Institute of Techology (KIT), Karlsruhe, Germany
[3]École Polytechnique Fédérale de Lausanne (EPFL), Swiss Plasma Center (SPC), CH-1015 Lausanne, Switzerland

[a]Author to whom correspondence should be addressed: ipagonakis@ethz.ch

ABSTRACT

Efficiency is a key factor for high-power gyrotrons, particularly in future fusion power plants, where a large number of gyrotron units will be required for plasma heating. A single-stage depressed collector enhances efficiency from approximately 35% to 50% by applying a decelerating potential to the spent beam electrons before they enter the collector. Experimentally, a well-defined threshold exists for the applied deceleration potential, beyond which efficiency decreases and instabilities arise. In this work, we conduct a systematic study of electron beam behavior under very high decelerating potentials by simulating the beam within the complete gyrotron geometry. This approach enables a comprehensive investigation of reflected electron behavior and its impact on cavity interactions. The findings provide insights into the limitations of single-stage depressed collectors. Moreover, quantifying the level of reflected current that does not significantly affect gyrotron performance is a key parameter for the design and development of high-efficiency multi-stage depressed collectors.

I. INTRODUCTION

A gyrotron is a vacuum tube designed to generate microwaves from an electron beam.[1] This device has found applications in plasma heating in nuclear fusion,[2–6] dynamic nuclear polarization in magnetic resonance,[7,8] and potentially in microwave-based hole drilling for geothermal applications.[9]

In gyrotrons, electrons are emitted via thermionic emission from an emitter ring mounted on the cathode. Electrons are then accelerated by an accelerating voltage V_{acc} applied between the cathode and the anode. Under the influence of a strong externally applied magnetic field, the electrons are guided into the interaction cavity, forming an electron beam. Within the cavity, the beam electrons transfer energy to a transverse electric microwave mode. A quasi-optical system converts the microwaves into a Gaussian mode, which is directed out of the gyrotron through a window. Meanwhile, the spent electron beam reaches the collector, where its residual energy is dissipated as heat. The efficiency η_{tot} of the gyrotron is defined as the ratio of the microwave output power P_{out} to the electrical power used for electron beam acceleration, which is defined as

$$\eta_{tot} = \frac{P_{out}}{I_b V_{acc}}, \tag{1}$$

where P_{out} is the microwave output power, and I_b is the beam current. In high-power gyrotrons, the efficiency typically reaches around 30%[3] and primarily depends on the interaction efficiency, ohmic losses, and stray radiation, which together determine the output power P_{out}.

A widely adopted method to enhance efficiency by approximately 50%[3,4] is the use of a single-stage depressed collector system. In this approach, a decelerating voltage V_{dec} is applied to recover part of the spent beam's kinetic energy before it reaches the collector. Consequently, the efficiency of the gyrotron can be expressed as

$$\eta_{tot} = \frac{P_{out}}{I_b(V_{acc} - V_{dec})}, \tag{2}$$

since the decelerating field reduces the electrical power required for gyrotron operation. From this equation, it is evident that increasing the decelerating voltage continuously improves efficiency. However, a fundamental limitation becomes evident in experimental campaigns involving gyrotrons with depressed collectors. When the decelerating

voltage exceeds a threshold associated with the slowest electrons in the energy distribution of the spent beam, these electrons are reflected back into the cavity, affecting the cavity interaction and the generated microwave power.[1,10,11] The location at which beam deceleration occurs significantly influences the optimal value of the decelerating voltage, as demonstrated through both theoretical and experimental investigations.[12] Therefore, it is generally assumed that the optimal efficiency of a gyrotron is achieved when no spent beam electrons are reflected, which defines the *slowest electron criterion.*

Reflected electrons appear not only in single-stage depressed collectors but also in multi-stage depressed collectors. Such systems are important for large-scale gyrotron operations, such as in nuclear fusion, to improve gyrotron efficiency, reducing electricity costs and complexity of cooling. A concept widely used for the separation of electron trajectories onto the different collection electrodes in theoretical designs is the $E \times B$ drift.[13] As a result, efficiencies exceeding 80% can be achieved.[14–17] In simulations of these designs, a small reflected current, on the order of a few tens to hundreds of milliamperes, is observed, however, raising concerns about its influence on the operation of multi-stage depressed collector gyrotrons.

The study of reflected electrons' behavior and their impact on cavity interaction and overall gyrotron performance is a numerically challenging problem. A fully accurate analysis requires a particle-in-cell (PIC) approach combined with multimode simulations of the cavity. However, this methodology is extremely time-consuming and demands a multiphysics framework that integrates both PIC-based cavity interaction models and PIC-based electron optics simulations. This complexity may explain why, to the best of our knowledge, there are no comprehensive studies in the literature that address this issue in detail. In the paper that first introduced the concept of applying a depressed collector to gyrotrons,[18] the behavior of reflected electrons is briefly mentioned, but no further analysis or modeling details are provided.

In this work, the behavior of reflected electrons is investigated in the context of a fusion gyrotron design featuring a single-stage depressed collector. The study provides insights into how reflected electrons affect the cavity interaction, power generation, and overall interaction efficiency.

To this end, the electron optics code *Ariadne* has been used to simulate the electron beam within the complete gyrotron geometry,[19] incorporating the cavity interaction based on a fixed-profile approximation approach. Further details on the methodology used in this study are provided in Sec. II, while Sec. III discusses the impact of reflected electrons on the gyrotron performance and efficiency. Finally, in Sec. IV, we summarize our findings and evaluate the validity of the slowest electron criterion.

II. NUMERICAL MODEL

Recently, a simulation model of the electron beam in the full gyrotron geometry, utilizing an electron optics code such as *Ariadne*, was proposed.[19] Based on this numerical model, the electron beam properties can be computed from the emitter, where electrons are generated, to the collector, where they are gathered. The effects of the electromagnetic field of the nominal transverse electric mode in the cavity are also taken into account using a fixed-profile approximation. To demonstrate this approach, the study used the geometry of a high-power dual-frequency gyrotron used for electron cyclotron resonance heating in the Tokamak à Configuration Variable (TCV) and operated at 126 GHz in the $TE_{26,7}$ mode.[20] The nominal operating parameters of the gyrotron are summarized in Table I, while a schematic overview of the complete design is presented in our previous work.[19]

As a continuation of this work, the simulation of the electron beam within the complete gyrotron geometry is extended to operating conditions where the deceleration of the spent beam exceeds the value defined by the *slowest electron criterion.* This leads to partial reflection of the electron beam. The objective is to investigate the behavior of the reflected electrons and their impact on cavity interaction, generated power, and overall gyrotron efficiency.

The convergence of the generated power with respect to the iteration number is presented in Fig. 1 for three operating points with deceleration voltages of 20, 22, and 24 kV. During the first ten iterations, simulations were performed in the absence of the electromagnetic field of the nominal mode. From iteration #10 to #20, the amplitude of the mode was gradually increased in a controlled manner, after which the amplitude was held constant for the following five iterations. Subsequently, a self-consistent simulation was conducted, ensuring that the output power from the cavity matched the beam power losses from the cavity entrance to its exit. In the absence of reflected electrons, as in the case of $V_{dec} = 20$ kV, the output power smoothly converges. However, this is not the case when the decelerating voltage increases, leading to partial reflection of beam electrons. As shown in Fig. 1, for $V_{dec} = 22$ kV, although the results are not dramatically altered, noticeable noise appears in the output power. Remarkably, for a slightly higher deceleration voltage of $V_{dec} = 24$ kV, the output power oscillates over a large range, even reaching negative values, which corresponds to an unphysical scenario where the electron beam extracts energy from the mode. This behavior arises because the electron optics code does not operate as a PIC simulation but instead follows a tracking approach. In particular, the updates of the static electric field and the cavity mode amplitude in each iteration take into account the complete set of trajectories of both the main beam and the reflected electrons. As a result, the beam parameters and the amplitude of the nominal mode can exhibit substantial fluctuations between successive iterations.

To address this issue without resorting to the computationally expensive PIC approach, the concept of a *relaxation factor* f_{rel} has been introduced. Specifically, to ensure a smooth transition between successive iterations, the contribution of the beam space charge in the calculation of the updated static electric field (obtained by solving the Poisson equation using the finite element method), as well as the amplitude of the mode in the cavity, are adjusted in a controlled manner between iterations.

In particular, at each iteration, the load vector,[21] which depends on the space charge of the electron beam, is updated as

$$\mathbf{b}_i = (1 - f_{rel}) \cdot \mathbf{b}_{i-1} + f_{rel} \cdot \mathbf{b}_i^*, \tag{3}$$

where $\mathbf{b}_{i-1}$ is the load vector from the previous iteration, $\mathbf{b}_i^*$ represents the load vector derived from the electron trajectories of the current iteration, while $\mathbf{b}_i$ is the load vector used for updating the static electric field in the current iteration i. In the finite element formulation of the

TABLE I. Operational parameters for the electron optics simulation.

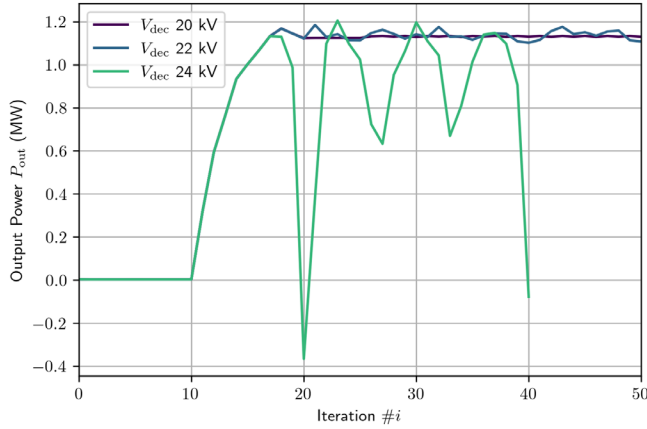| Operating mode	$TE_{26,7}$
Frequency f	126 GHz
Magnetic field B_{cvt}	5 T
Beam current I_b	40 A
Accelerating voltage V_{acc}	83.3 kV
Output power P_{out}	1.14 MW

FIG. 1. Output power P_{out} in the absence of relaxation factors for increasing decelerating voltages V_{dec}.

Poisson equation, the load vector is constructed from the volume integral of the space charge density weighted by the interpolation functions, thereby capturing the influence of the space charge distribution on the electrostatic potential field. Additionally, the effect of Dirichlet boundary conditions (or, equivalently, the voltage applied to the gyrotron's electrodes) is incorporated by the prescribed potential values directly, ensuring that the solution adheres to the specified potential on the domain boundaries.

A similar equation is also applied to the amplitude of the mode in the cavity, given by

$$V_i = (1 - f_{rel}) \cdot V_{i-1} + f_{rel} \cdot V_i^*, \tag{4}$$

where V_{i-1} is the mode amplitude from the previous iteration, V_i^* represents the mode amplitude derived from the beam power losses in the current iteration, while V_i is the mode amplitude used for updating the beam trajectories in the next iteration. The algorithm in pseudo-code is as follows:

$\nabla^2\phi = 0 \rightarrow \mathbf{M}\varphi = \mathbf{b}_0 \rightarrow \boldsymbol{E}_s$
for $i \leftarrow 1$ to N **do**
  if $i \leq N_a$ **then**
    $V_i = 0$
  else if $i \leq N_b$ **then**
    $V_i = V_{max}(i - N_a)/(N_b - N_a)$
  else if $i \leq N_c$ **then**
    $V_i = V_{max}$
  else
    $V_i^* = \sqrt{\Delta P_{beam}/G}$
    $V_i = (1 - f_{rel}) \cdot V_{i-1} + f_{rel} \cdot V_i^*$
  else if
    $\dfrac{d\boldsymbol{p}}{dt} = -e\big\{[\boldsymbol{E}_s + \boldsymbol{E}_m(V_i)] + \boldsymbol{v} \times [\boldsymbol{B}_s + \boldsymbol{B}_m(V_i)]\big\}$
    $\rightarrow (\rho, \Delta P_{beam})$
  $\mathbf{b}_i = (1 - f_{rel}) \cdot \mathbf{b}_{i-1} + f_{rel} \cdot \mathbf{b}_i^*(\varrho)$
  $\nabla^2\phi = -\dfrac{\rho}{\epsilon_0} \rightarrow \mathbf{M}\varphi = \mathbf{b}_i \rightarrow \boldsymbol{E}_s$
end for

In the pseudo-code, the equation $\mathbf{M}\varphi = \mathbf{b}_i$ represents the linear system derived from the finite element formulation of the Poisson equation. Here, $\mathbf{M}$ is the stiffness matrix, and φ is the vector of unknowns containing the electric potential ϕ at the nodes of the mesh used to discretize the geometry domain. The vector $\mathbf{b}_0$ corresponds to the load vector that accounts only for the Dirichlet boundary conditions, while $\mathbf{b}_i$ includes both the boundary conditions and the contribution from the space charge, as previously described. $\boldsymbol{E}_s$ and $\boldsymbol{B}_s$ are the static electric and magnetic fields, respectively, $\boldsymbol{E}_m$ and $\boldsymbol{B}_m$ are the electric and magnetic fields of the nominal mode, N is the total number of iterations, V_{max} is the nominal field amplitude of the microwave mode, ΔP_{beam} is the power loss of the beam, and G is a normalization factor. For more information, the reader is referred to our previous study.[19] In this study, the various phases of the simulation are set to lengths of $N_a = 10$, $N_b = 10$, $N_c = 5$, and $N_d = 975$.

The relaxation factor f_{rel} takes values between 0 and 1. When $f_{rel} = 1$, the simulation follows the standard tracking approach, where the electron beam trajectories of the previous iteration exclusively determine the load vector, and the beam losses of the previous iteration define the amplitude of the nominal mode in the cavity. Conversely, using smaller values of the relaxation factor reduces the influence of the current electron beam state on the space charge array, allowing only small changes in the static electric field and the mode amplitude in the cavity. However, the smaller the relaxation factor, the more iterations are required to achieve convergence to a stable and physically reasonable result.

III. NUMERICAL RESULTS

A. Convergence and relaxation factors

The convergence of the output power was systematically investigated for different values of the relaxation factor for a high value of the decelerating voltage, $V_{dec} = 36$ kV, as shown in Fig. 2.

At $f_{rel} \geq 0.5$, the simulation may crash due to instabilities between the successive iterations. For $f_{rel} = 0.4$, we see irregular oscillation of the output power P_{out}. This oscillation disappears at $f_{rel} = 0.1$ where a converged output is observed already before 100 iterations have passed. Decreasing the relaxation factor further increases the number of iterations until convergence is achieved. It is worth noting
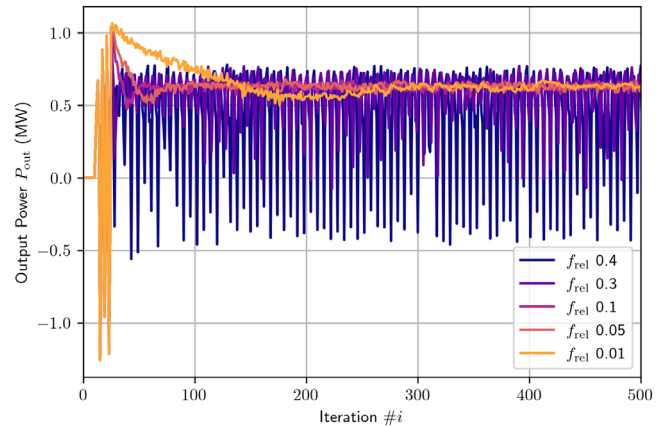

FIG. 2. Evolution of output power with iterations for different relaxation factors at $V_{dec} = 36$ kV. The simulations fail at $f_{rel} \geq 0.5$. Significant oscillations commence at $f_{rel} = 0.3$.
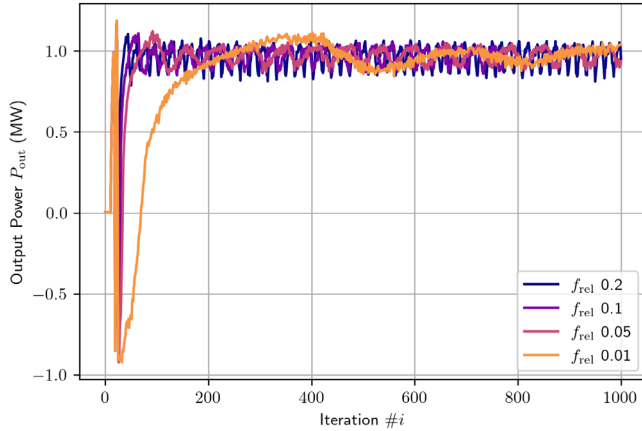
FIG. 3. Evolution of output power with iterations for different relaxation factors at $V_{dec} = 26$ kV.

that the solution to which the output power converges is independent of the choice of relaxation factor.

The convergence behavior of the parameters varies for different decelerating voltages. For certain values of the decelerating voltage, such as $V_{dec} = 26$ kV, instead of stabilizing at a single value, the solution oscillates between two distinct values, as shown in Fig. 3. Reducing the relaxation factors increases the oscillation period in terms of iterations count, but the maximum and minimum values remain nearly unchanged. This oscillatory behavior is inherently linked to the dynamic nature of the phenomenon, which cannot be fully captured by the simplified model used in this work.

Convergence of the output power P_{out} at varying deceleration voltages is summarized in Fig. 4. The variation, given by the difference of the max and min values, was calculated over the last 300 iterations. The convergence, here depicted as the output power variation ΔP_{out}, improves with decreasing relaxation factors, especially for higher decelerating voltages. Below $f_{rel} = 0.2$, the results have converged for both voltages, with consistent means and absolute standard deviations. Consequently, $f_{rel} = 0.1$ was chosen for all subsequent simulations.

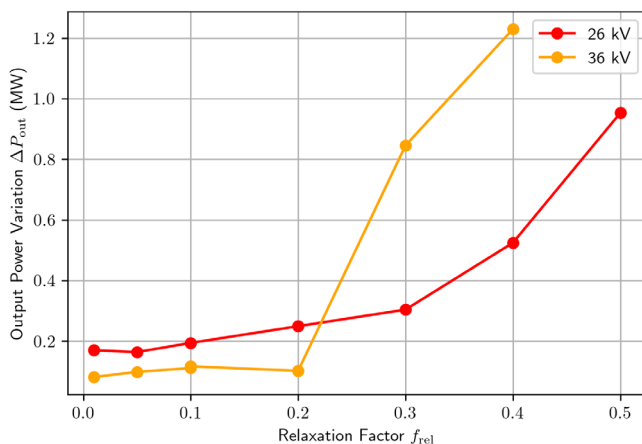### B. Reflected electron statistics

When the decelerating voltage exceeds a certain threshold, a fraction of the spent beam electrons with low kinetic energy are reflected backward toward the cavity. These electrons become electrostatically trapped in a potential well, formed between the cathode and the deceleration region of the spent beam, causing them to oscillate between these two axial positions. The electromagnetic field in the cavity influences their kinetic energy, leading to either energy gain or loss with each passage through the cavity, thereby impacting the overall interaction efficiency. After multiple oscillations, the trapped electrons eventually acquire sufficient energy to escape the potential well. In other words, the electromagnetic field in the cavity acts like a pump, driving the electrons out of the electrostatic trap.[18,22]

For the decelerating voltage values used in this study, most electrons are not reflected and are instead directly collected at the collector, as illustrated in Fig. 5. Herein, the minimum number of passings of an electron through the center of the cavity is shown. All 500 macro-electrons with 20 phases each, amounting to 10 000 electrons total, pass the cavity once. We refer to the large fraction of electrons that are then collected as the initial electron beam. The remaining electrons are reflected back toward the cathode, of which the majority is reflected back toward the collector. A large fraction is collected there as a subset of electrons is reflected once more, until, after several iterations, all electrons are collected.

At $V_{dec} = 21$ kV no reflections are observed, while already at 22 kV up to seven passings through the cavity (or six reflections) are recorded. With increasing decelerating voltage, both the number of reflected electrons and the number of reflections for each electron increase; hence, the fraction collected at the collector and cathode at each opportunity decreases. It is clear that the probability of an electron being collected at the electron gun is significantly lower than the probability of collection at the collector. The electrode collection has been fit to the formula

$$N_l = N_0 e^{-a_{col}\lceil(l-1)/2\rceil} e^{-a_{cat}\lfloor(l-1)/2\rfloor}, \qquad (5)$$

where N_l is the number of electrons not yet collected, l is the index specifying the number of passings through the cavity, $\lceil \ \rceil$ is

FIG. 4. Variation range of the mean output power ΔP_{out} as a function of relaxation factor at different deceleration voltages.
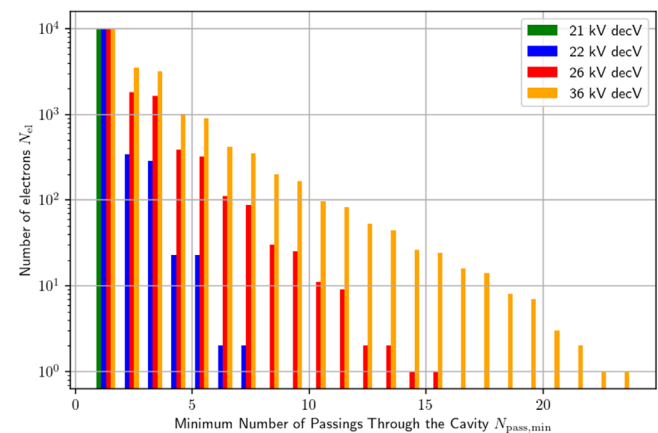

FIG. 5. Number of electrons that have passed the cavity at least N_{pass} times for various decelerating voltages.

the ceiling function, and $\lfloor \rfloor$ is the floor function. At $l = 1$, the original $N_0 = 10000$ electrons are present. N_l then decreases stepwise, with large decreases whenever the electrons reach the collector due to the large collector collection coefficient a_{col} and small steps whenever the electrons reach the cathode due to the small cathode collection coefficient a_{cat}. A table of the fitted parameters to the multi-exponential decay of reflected electrons is given in Table II.

For $V_{dec} = 21$ kV, no collection coefficients were evaluated as no reflections occurred. Note that the value of a_{cat} at 22 kV is negative, which would indicate emission of (secondary) electrons at the cathode. The simulation is unable to simulate such an effect, and we consider the negative value an artifact of the model.

The dependence of the collected current at the cathode and the collector on the decelerating voltage is given in Fig. 6. The error bars depict the absolute standard deviation of the sampled forward and reverse currents. The *slowest electron criterion* is indicated by the vertical black line. Currents collected at the collector i_{col} and cathode i_{cat} make up the entire beam current, as no electrons were found permanently trapped in the cavity over the studied range of deceleration voltages. i_{col} increases approximately linearly, as i_{cat} decreases accordingly, with increasing decelerating voltage.

Since electrons constituting i_{cat} will likely arrive at the emitter ring with residual kinetic energy, secondary electron emission and cathode overheating are likely.[23–26] These effects have not been considered in this study; however, they may have additional detrimental effects on gyrotron operation (even if secondary electrons are not emitted at the electron gun[27]) and electron gun longevity.

Forward and reverse currents i_{for} and i_{ref} are defined as the current of all electrons in the center of the cavity with a positive and negative dimensionless momentum u_z, respectively. Both currents increase proportionally to decelerating voltage applied above 21 kV, leading to a significant reflected current that amounts to 50% of the initial forward directed current at $V_{dec} = 36$ kV, far exceeding the milliamperes of current observed in other studies.[14,15] The convergence of these values is poorer around $V_{dec} = 26$ kV, as the parameters consistently oscillated as seen in Fig. 3.

C. Power and efficiency

As expected, the presence of reflected electrons affects the operation of the gyrotron in multiple ways. First, as these electrons pass through the cavity, they interact with the electromagnetic fields of the nominal mode excited in the cavity. Most of these electrons gain energy from the mode, which eventually enables them to escape the potential well formed between the cathode and the deceleration region
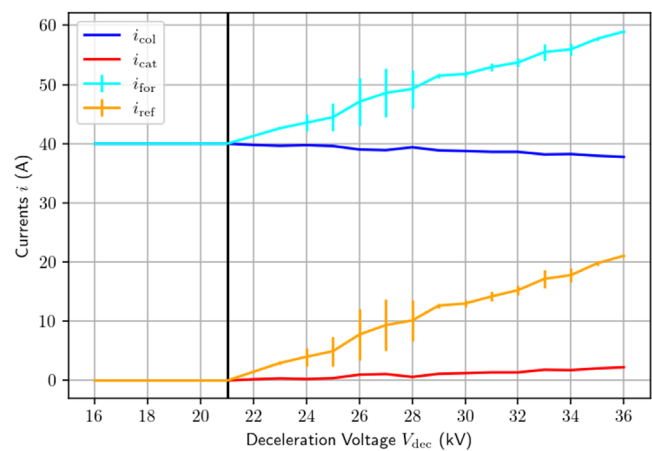

FIG. 6. Currents collected on the collector i_{col} and cathode i_{cat} as well as forward i_{for} and reflected i_{ref} current measured in the gyrotron cavity center as a function of decelerating voltage.

of the spent beam, as discussed earlier. This process impacts the generated microwave power of the gyrotron. Additionally, the space charge of the reflected electrons in the gun region alters the properties of the initial beam, further deteriorating the performance of the cavity interaction.

The model used to investigate this pathological gyrotron operation is based on the fixed-profile approximation. Specifically, it assumes that the presence of reflected electrons influences the amplitude of the axial profile of the nominal mode while keeping its shape, as well as the phase and the operating frequency, unchanged. This is a rough approximation, as in reality, the profile shape, the phase, and the operating frequency of the mode could be significantly modified due to the presence of reflected electrons. Furthermore, mode competition could lead to mode loss. A more realistic simulation will be the subject of future work, utilizing the recently developed cavity interaction code *Phaedra*.[28]

Using the electron beam simulation in the overall gyrotron geometry, important information about the deterioration of the electron beam at the cavity entrance due to the presence of the reflected electrons was extracted. First, the space charge of these electrons causes an additional voltage depression on the electron beam, which causes a significant decrease in the initial beam kinetic energy. As shown in Fig. 7, increasing the decelerating voltage causes a significant shift toward lower energy in the kinetic energy probability distribution.

The space charge of the reflected electrons reduces the electric field on the emitter ring surface, leading to a slight reduction in the average pitch factor of the electron beam at the cavity entrance, as illustrated in Fig. 8. Error bars depict the absolute standard deviation, and triangles depict the minimum ($\triangle$) and maximum ($\triangledown$) values. All values were calculated over the last 300 iterations of the simulation. The beam degradation is also quantified by a significant increase in the transverse velocity spread at the cavity entrance. Specifically, in the absence of reflected electrons at decelerating voltages of 21 kV and less, the velocity spread remains below 2%. However, it rises sharply at the onset of reflected electrons and exceeds 20% for decelerating voltages above 27 kV.

TABLE II. Fit of collection coefficients and fractions of electrons collector at the collector and cathode, respectively. For $V_{dec} = 21$ kV, no parameters were evaluated as no reflections occurred. Note that the negative value of a_{cat} at 22 kV is a result of imperfect fitting; the simulation does not consider secondary electron emission.

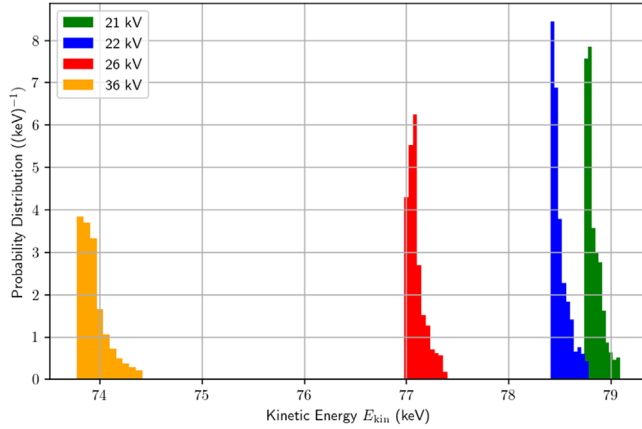| V_{dec}	a_{col}	a_{cat}	Collector fraction	Cathode fraction
21 kV	$\cdots$	$\cdots$	100%	0%
22 kV	3	-0.08	99.5%	0.5%
26 kV	1.2	0.05	97.5%	2.5%
36 kV	0.7	0.09	94.3%	5.7%

FIG. 7. Kinetic energy probability distribution of the initial electron beam, excluding any reflected electrons, at the cavity entrance for various decelerating voltages.

The degradation of the electron beam has a strong effect on the generated power and efficiency, as shown in Figs. 9 and 10, respectively. In the absence of reflected electrons, a stable output power of $P_{out} = 1.13$ MW at the cavity exit is reached. The power starts dropping sharply, soon after the onset of reflected electrons.

From the generated output power, the electronic efficiency $\eta_{ele} = P_{gen}/(I_b V_{acc})$ can be calculated, neglecting voltage depression, where P_{gen} is the generated microwave power in the cavity.

The drop in output power is a direct result of the decrease in electronic efficiency η_{ele}, see Fig. 10. In the absence of reflected electrons, η_{ele} is independent of V_{dec}, while the collector efficiency $\eta_{col} = V_{dec}/(V_{acc}(1 - \eta_{ele}))$ increases, leading to an increase in the overall efficiency. At 23 kV, the reflected electrons cause the electronic efficiency to plummet and the collector efficiency to grow more slowly, leading to a decrease in the overall efficiency.

Interestingly, at 22 kV, where the first reflected electrons have already appeared, η_{ele} is still stable. It is remarkable that the electronic efficiency in the absence of reflected electrons is in the same range as it is experimentally estimated at around 36%.[29] The TCV gyrotron of
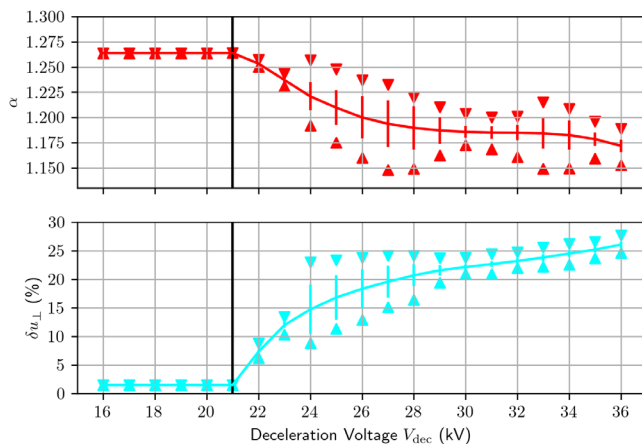

FIG. 8. Pitch factor α (top) and dimensionless perpendicular momentum spread $\delta u_\perp$ (bottom) as a function of V_{dec} of all electrons at the entrance of the cavity.
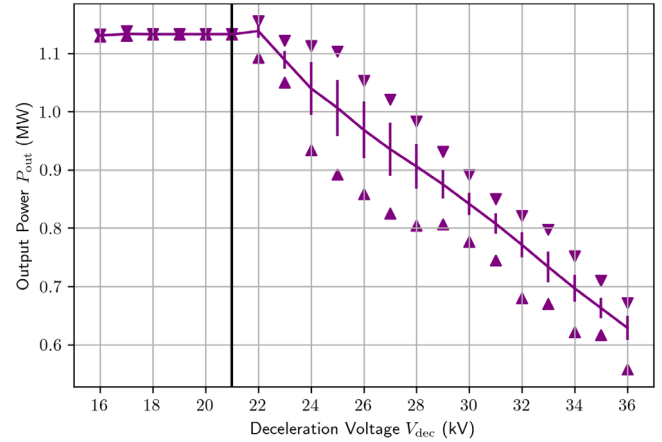

FIG. 9. Output power P_{out} changing as a result of applied decelerating voltage V_{dec}.
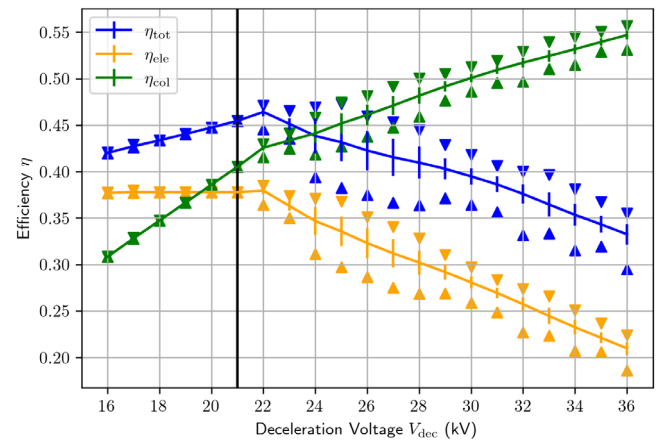

FIG. 10. Change in electronic, collector, and total efficiency with increasing decelerating voltage. Ohmic losses of 10% have been assumed for the total efficiency.

that study does not have a depressed collector. Here, we find the highest overall efficiency of 46%, which is slightly short of the desired 50% estimated in the same study with a single-stage depressed collector.

The highest overall efficiency in our study is at $V_{dec} = 22$ kV, a slightly higher operating point than what is determined by the *slowest electron criterion*.

IV. CONCLUSION

The behavior of reflected electrons in a gyrotron is investigated. This is a numerically complex and computationally demanding problem. Ideally, PIC simulations would be required to resolve the electron dynamics, along with a multi-mode analysis to evaluate the impact of reflected electrons on mode stability. However, this approach is highly resource-intensive and time-consuming.

To address the problem more efficiently, a simplified method is adopted based on a set of approximations. An electrostatic tracking code is used to compute the trajectories and static self-fields of both the main electron beam and the reflected electrons. The electromagnetic field profile of the cavity mode is defined using the fixed-field

approximation. Instead of simulating the full-time evolution of the system, relaxation factors are applied to estimate the time-averaged effects of the reflected electrons on gyrotron operation, assuming stable operation of the nominal mode. Such simulation for each operating point requires approximately one to two days of computation time, using the high-performance computing facilities at ETH Zurich.[30]

The behavior of the reflected electrons has been thoroughly examined. Most of these electrons gain energy from the electromagnetic mode within the cavity and, after multiple reflections, eventually reach the collector wall. However, a small fraction of them reach the cathode surface, potentially causing overheating of the emitter ring and triggering secondary electron emission effects that are not considered in this analysis.

Reflected electrons can have a profound impact on gyrotron operation. Specifically, the quality of the electron beam deteriorates significantly, affecting interaction efficiency. Additionally, the energy gained by reflected electrons from the electromagnetic fields in the cavity strongly influences both the output power and overall efficiency.

The highest efficiency is observed at a deceleration voltage slightly higher than the threshold proposed. Nonetheless, the *slowest electron criterion* should be used to determine the optimal decelerating voltage, as additional detrimental effects were not considered here.

Furthermore, a key conclusion is that, according to this model, the generated power is not significantly affected by reflected current less than one ampere. This finding is particularly important for the development of multi-stage depressed collector systems, where a small fraction of the current may be reflected.[14]

AUTHOR DECLARATIONS
Conflict of Interest

The authors have no conflicts to disclose.

Author Contributions

Lea Marti: Conceptualization (equal); Data curation (equal); Formal analysis (equal); Investigation (equal); Methodology (equal); Resources (equal); Visualization (equal); Writing – original draft (equal); Writing – review & editing (equal). **Ioannis Gr. Pagonakis:** Conceptualization (lead); Data curation (supporting); Formal analysis (lead); Investigation (equal); Methodology (equal); Project administration (lead); Software (lead); Validation (lead); Visualization (supporting); Writing – original draft (equal); Writing – review & editing (equal). **Chieh-Lin Chiang:** Data curation (supporting); Investigation (supporting); Writing – review & editing (supporting). **Chuanren Wu:** Conceptualization (supporting); Writing – review & editing (supporting). **Jérémy Genoud:** Formal analysis (supporting); Resources (supporting); Writing – review & editing (supporting). **Marthe Millen:** Resources (supporting); Writing – review & editing (supporting). **Jean-Philippe Hogge:** Formal analysis (supporting); Resources (equal); Writing – review & editing (supporting). **Alexander B. Barnes:** Funding acquisition (lead); Project administration (supporting); Writing – review & editing (supporting).

DATA AVAILABILITY

The data that support the findings of this study are available from the corresponding author upon reasonable request.

REFERENCES

[1] A. S. Gilmour, *Klystrons, Traveling Wave Tubes, Magnetrons, Cross-Field Amplifiers, and Gyrotrons* (Artech House, 2011).

[2] G. Gantenbein, V. Erckmann, S. Illy, S. Kern, W. Kasparek, C. Lechte, W. Leonhardt, C. Liévin, A. Samartsev, A. Schlaich, M. Schmid, and M. Thumm, J. Infrared. Milli. Terahz. Waves **32**, 320 (2011).

[3] I. G. Pagonakis, F. Albajar, S. Alberti, K. Avramidis, T. Bonicelli, F. Braunmueller, A. Bruschi, I. Chelis, F. Cismondi, G. Gantenbein, V. Hermann, K. Hesch, J. P. Hogge, J. Jelonnek, J. Jin, S. Illy, Z. C. Ioannidis, T. Kobarg, G. P. Latsas, F. Legrand, M. Lontano, B. Piosczyk, Y. Rozier, T. Rzesnicki, A. Samartsev, C. Schlatter, M. Thumm, I. G. Tigelis, M. Q. Tran, T. M. Tran, J. Weggen, and J. L. Vomvoridis, Fusion Eng. Des. **96–97**, 149 (2015).

[4] K. Sakamoto, A. Kasugai, K. Takahashi, R. Minami, N. Kobayashi, and K. Kajiwara, Nat. Phys. **3**(6), 411 (2007).

[5] J. F. Tooker, P. Huynh, K. Felch, M. Blank, P. Borchardt, and S. Cauffman, Fusion Eng. Des. **88**, 521 (2013).

[6] V. E. Zapevalov, G. G. Denisov, V. A. Flyagin, A. S. Fix, A. N. Kuftin, A. G. Litvak, M. V. Agapova, V. N. Iljin, V. A. Khmara, V. E. Myasnikov, V. O. Nichiporenko, L. G. Popov, S. V. Usachev, V. V. Alikaev, and V. I. Iljin, Fusion Eng. Des. **53**, 377 (2001).

[7] L. R. Becerra, G. J. Gerfen, R. J. Temkin, D. J. Singel, and R. G. Griffin, Phys. Rev. Lett. **71**, 3561 (1993).

[8] F. J. Scott, E. P. Saliba, B. J. Albert, N. Alaniva, E. L. Sesti, C. Gao, N. C. Golota, E. J. Choi, A. P. Jagtap, J. J. Wittmann, M. Eckardt, W. Harneit, B. Corzilius, S. Th. Sigurdsson, and A. B. Barnes, J. Magn. Reson. **289**, 45 (2018).

[9] P. Woskov and D. Cohn, "Annual report 2009: Millimeter wave deep drilling for geothermal energy, natural gas and oil MITEI seed fund program," Technical Report (Massachusetts Institute of Technology, 2009).

[10] H. G. Kosmahl, Proc. IEEE **70**, 1325 (1982).

[11] H. G. Kosmahl and P. Ramins, IEEE Trans. Electron Devices **ED-24**, 36 (1977).

[12] I. G. Pagonakis, S. Illy, Z. C. Ioannidis, T. Rzesnicki, K. A. Avramidis, G. Gantenbein, T. Kobarg, B. Piosczyk, M. Thumm, and J. Jelonnek, IEEE Trans. Electron Devices **65**, 2321 (2018).

[13] I. G. Pagonakis, J. P. Hogge, S. Alberti, K. A. Avramides, and J. L. Vomvoridis, IEEE Trans. Plasma Sci. **36**, 469 (2008).

[14] B. Ell, I. G. Pagonakis, C. Wu, M. Thumm, and J. Jelonnek, Phys. Plasmas **26**, 113107 (2019).

[15] B. F. Ell, C. Wu, G. Gantenbein, S. Illy, M. S. Misko, I. G. Pagonakis, J. Weggen, M. Thumm, and J. Jelonnek, IEEE Trans. Electron Devices **70**, 1299 (2023).

[16] V. N. Manuilov, M. V. Morozkin, O. I. Luksha, and M. Y. Glyavin, Infrared Phys. Technol. **91**, 46 (2018).

[17] O. I. Louksha, A. G. Malkin, and P. A. Trofimov, IEEE Electron Device Lett. **45**, 1638 (2024).

[18] K. Sakamoto, M. Tsuneoka, A. Kasugai, T. Imai, T. Kariya, K. Hayashi, and Y. Mitsunaka, Phys. Rev. Lett. **73**, 3532 (1994).

[19] L. Marti, I. G. Pagonakis, L. Sieben, M. Millen, J. Genoud, J.-P. Hogge, and A. B. Barnes, Phys. Plasmas **31**, 103102 (2024).

[20] J.-P. Hogge, S. Alberti, K. A. Avramidis, A. Bruschi, W. Bin, F. Cau, F. Cismondi, J. Dubray, D. Fasel, G. Gantenbein, S. Garavaglia, J. Genoud, T. P. Goodman, S. Illy, J. Jin, F. Legrand, R. Marchesin, B. Marlétaz, J. Masur, A. Moro, C. Moura, I. G. Pagonakis, E. Périal, L. Savoldi, T. Scherer, U. Siravo, M. Thumm, M. Toussaint, and M.-Q. Tran, *AIP Conference Proceedings* (AIP Publishing LLC, 2020), p. 090006.

[21] S. S. Rao, *The Finite Element Method in Engineering* (Elsevier, 2010).

[22] I. G. Pagonakis, B. Piosczyk, J. Zhang, S. Illy, T. Rzesnicki, J. P. Hogge, K. Avramidis, G. Gantenbein, M. Thumm, and J. Jelonnek, Phys. Plasmas **23**, 23105 (2016).

[23] G. A. Harrower, Phys. Rev. **104**, 52 (1956).

[24] A. Shih and C. Hor, IEEE Trans. Electron Devices **40**, 824 (1993).

[25] H. Bruining, Phys. Appl. Secondary Electron Emission **1962**, 27–51 (1962).

[26] M. A. Furman and M. T. Pivi, Phys. Rev. Spec. Top. Accel. Beams **5**, 82 (2002).

[27] S. Cauffman, M. Blank, P. Borchard, and K. Felch, *2020 IEEE 21st International Conference on Vacuum Electronics, IVEC* (IEEE, 2020), p. 189.

[28] I. G. Pagonakis and A. B. Barnes, Appl. Math. Modell. **147**, 116194 (2025).

[29] S. Alberti, K. A. Avramidis, W. Bin, A. Bertinetti, J. Dubray, D. Fasel, S. Garavaglia, J. Genoud, T. Goodman, J. P. Hogge, P. F. Isoz, P. Lavanchy, F. Legrand, B. Marletaz, J. Masur, A. Moro, I. G. Pagonakis, M. Silva, U. Siravo, and M. Toussaint, *International Conference on Infrared, Millimeter, and Terahertz Waves, IRMMW-THz 2019-September* (2019).

[30] ETH Zürich, https://scicomp.ethz.ch/wiki/Euler.